IEEE Access
Multidisciplinary ⋮ Rapid Review ⋮ Open Access Journal

Received August 13, 2020, accepted August 31, 2020, date of publication September 9, 2020, date of current version September 24, 2020.

Digital Object Identifier 10.1109/ACCESS.2020.3022886

Piecewise Adaptive-Norm Trend Filtering Method for ICESat/GLAS Waveform Data Denoising

LIANYING LI, MENGRONG CAI, XIAOBIN GUAN, AND DONG CHU
School of Resource and Environmental Sciences, Wuhan University, Wuhan 430079, China

Corresponding author: Xiaobin Guan (guanxb@whu.edu.cn)

This work was supported in part by the National Key Research and Development Program of China under Grant 2018YFB1600600, in part by the Joint Funds of the National Natural Science Foundation of China under Grant U1764262, and in part by the LIESMARS Special Research Funding.

ABSTRACT The Geoscience Laser Altimeter System (GLAS) aboard Ice, Cloud and land Elevation Satellite (ICESat) was able to capture the full waveform of backscattered laser pulse. However, the accuracy of the surface information extracted from the waveform was vulnerable to background noise. In this paper, a piecewise adaptive l_q-*norm* trend filtering method is proposed for the GLAS full waveform denoising on the basis of trend filtering. To minimize the loss of useful signal while removing the noise, the proposed method adaptively assigns different norms to the smooth constraints according to the local signal energy. The filtered results can then be obtained by iteratively minimizing the hybrid-norm loss function. The proposed method is tested on both the simulated waveforms and real GLAS waveform data. In the simulated experiments, the quantitative evaluation is conducted with the filtered waveforms, as well as the results after waveform decomposition. For comparison, the most commonly used waveform filtering methods, i.e. Gaussian filtering, wavelet transform, Empirical model decomposition and l_1 trend filtering, are involved in the experiments. The results show that the proposed method outperforms the mainstream methods on waveform filtering, in terms of removing noise and preserving the shape and energy amplitude of the GLAS waveforms.

INDEX TERMS ICESat/GLAS, full waveform filtering, adaptive norm, signal processing.

I. INTRODUCTION

Ice, Cloud and land Elevation Satellite (ICESat), launched in 2003 by National Aeronautics and Space Administration (NASA) was designed to measure ice sheet mass balance, cloud and aerosol heights, as well as land topography and vegetation characteristics over the Earth's surface [1]. The Geoscience Laser Altimeter System (GLAS) onboard ICESat was the first space-borne laser-ranging instrument for global surface monitoring and has provided high-quality data relating to topography and cloud and atmospheric properties [2]. During the seven years on duty, ICESat GLAS has acquired LiDAR waveforms recording the vertical information of targets within footprints. The relative accuracy of its elevation measurement is confirmed to be about 15 cm over most of the ice sheet [3], [4]. Over land, the accuracy is better than one meter in low slope regions and up to 10 m in large slope regions [4]. The ICESat GLAS data has been used in a wide range of disciplines, including ice-elevation changes, sea-ice freeboard, forest canopy height, cloud heights and land-terrain changes [5]–[9] and still plays a part in the related researches in recent years [7], [10]–[12]. However, the shape of backscattered waveforms is vulnerable to background noise which is mainly composed of dark current noise and thermal noise [13]. This can lead to uncertainty in extracting the information of reflecting surface. Waveform denoising using a filtering method is an effective way to minimize the influence of the noise and improve the accuracy of measurement [14], [15].

At present, many filtering methods have been applied to GLAS waveform for noise removal, including frequency domain methods, spatial domain methods, and time-frequency based methods [13], [14], [16]–[19]. Among them, frequency domain methods are simple and easy to implement, which are the most commonly used category of methods. Iqbal *et al.* [20] employed the Fourier transform to filter GLAS waveform in the frequency domain. Jutzi and Stilla [14] used Wiener filtering to denoise

The associate editor coordinating the review of this manuscript and approving it for publication was Naveed Ur Rehman.

simulated waveform. Qiu *et al.* [18] performed the GLAS data filtering based on wavelet transform, and compared the performance of various wavelet basis on GLAS waveform. They came to the conclusion that the Symlets wavelet basis function is more suitable for GLAS data processing than the Daubechies basis. The frequency domain methods are effective in suppressing the high-frequency noise given that the frequency of the signal part in the waveform is typically lower than that of the noise. However, the performance of the frequency domain methods is not always satisfactory when the details of signal and noise are difficult to be completely distinguished in the frequency domain. Moreover, Wiener filtering can cause artificial oscillations around sharp edges [13].

There are also several attempts in developing spatial domain methods for waveform denoising, such as the Gaussian filtering [13], [21], Savitzky-Golay filtering [19], moving average filtering [22], exponential smoothing [23], Hodrick-Prescott (H-P) filtering [24] and l_1 trend filtering [25]. Compared with the frequency domain methods, the spatial domain methods can make more intuitive use of the characteristics of signal and noise. However, the main problem of current solutions is that it will smear the waveform while removing noise, especially in the signal peaks, therefore reducing the amplitude of the waveform. In addition, considering the non-linear and non-stationary property of Lidar signal, time-frequency based methods are suitable for its processing, such as Empirical Model Decomposition (EMD) and Synchrosqueezing trans-form [26]–[28]. Among them, EMD has been extensively applied in Lidar signal processing, which is a data-driven method can self-adaptively decomposes the original signal into several Intrinsic Model Functions. Noise reduction is achieved by removing the first few noisy components in the high-frequency components. However, this method may lead to obvious signal loss due to the useful information in the discarded components, so attempts are needed to further improve its performance [29], [30].

In essence, the filtering of GLAS waveform is consistent with the problem of 1-D signal denoising. The background noise should be removed as much as possible, while the useful signal needs to be preserved. To find the intrinsic smooth trend in terms of a given series, a large number of trend filtering methods have been proposed [22]–[25], [31]. Among them, H-P filtering and l_1 trend filtering are typical algorithms, which are developed based on the regularization theory [32]. The regularized framework aims to regularize the residual terms and the smoothness measurements of intrinsic trend, which is flexible and easy to understand. The residual term usually corresponds to the noise distribution, while the smoothness term depicts the variations in the trend. The l_1 trend filtering used l_1-*norm* to measure the smoothness of the estimated trend, so the estimated result is piecewise smooth and allows more signal details preserved [25]. However, the l_1-*norm* based constraints are prone to preserve unnecessary noisy signals in the cases with strong noise. On the contrary, the HP filtering algorithm, which use the constraints with the sum of squares (l_2-*norm*), usually can effective remove noise but easy to obtain over-smooth results with signals losses.

There are few studies have successfully employed the adaptive norms in the field of image denoising, and achieved desirable results [33], [34]. It could be an ideal solution to address the problems of the trade-off in the HP and l_1 trend filtering methods, which equips the capacity to balance the noise removal and signal preserving. However, the applicable of the adaptive norms in the 1-D trend filtering has not been proved yet. As a result, in order to overcome the shortcomings of traditional filtering methods and meet the requirements of GLAS waveform filtering, a piecewise adaptive l_q-*norm* trend filtering method is proposed in this paper. To minimize the loss of effective signal while removing the noise, different norms are assigned to the smooth constraints of the estimated signal according to the local signal energy. The filtered results can then be obtained by iteratively minimizing the hybrid-norm loss function. Simulated experiments and real data experiments are conducted to validate the effectiveness of the proposed method in GLAS waveform filtering. In the simulated experiments, the quantitative evaluation is obtained with the filtered waveforms, as well as the results after waveform decomposition.

II. DATA AND METHODOLOGY

In this section, the ICESat/GLAS data and its waveform simulation for quantitative experiments are first introduced. Then the structure and differences of HP filtering and l_1 trend filtering methods are presented. The proposed method is described at last, as well as the analysis about the relationship between its key parameter and different waveforms.

A. ICESat/GLAS DATA

GLAS measures the surface and atmosphere by transmitting 1064 nm Gaussian infrared light and 532 nm Gaussian visible green light respectively, and receiving the reflected echoes [1]. It provides 16 data products which are distributed by the National Snow and Ice Data Center (NSIDC) and can be downloaded freely. Among them, GLA01 is the original file to record the LiDAR echo, including the original waveform signal, noise mean, noise standard deviation, emission pulse waveform, longitude and latitude coordinates and beam number. As shown in Figure.1, the sample GLA01 waveform consists of 544 discrete photovoltaic values.

The waveforms from various surface types have different characteristics. Figure. 1(a) shows the signal from flat bare surface, thus there is only one narrow peak. Figure. 1(b) is a land surface echo with multiple peaks. The echo can be widened due to rough or inclined surface and multiple peaks are caused by obvious ground objects, e.g. vegetation and buildings [35]. The GLAS waveforms can be ideally decomposed into several signal components to obtain waveform parameters, such as the ground position, signal starting and end position and the effective waveform length [36]. For example, the waveform in Figure. 1(b) can be decomposed into three signal components after waveform filtering.

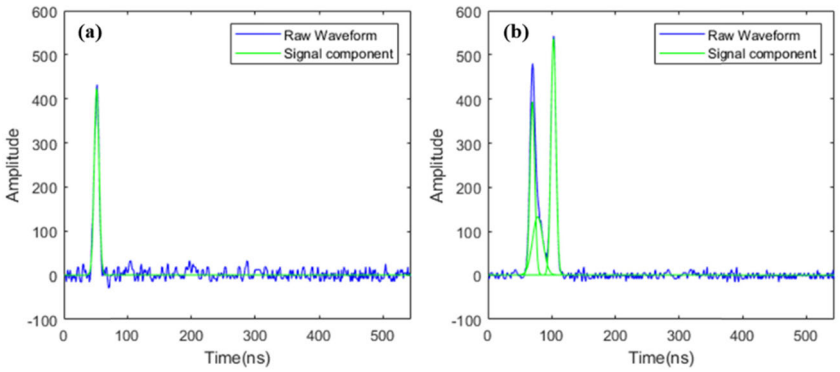

FIGURE 1. GLAS waveform examples for single peak (a) and multiple peaks (b), with raw waveform and decomposed signal components.

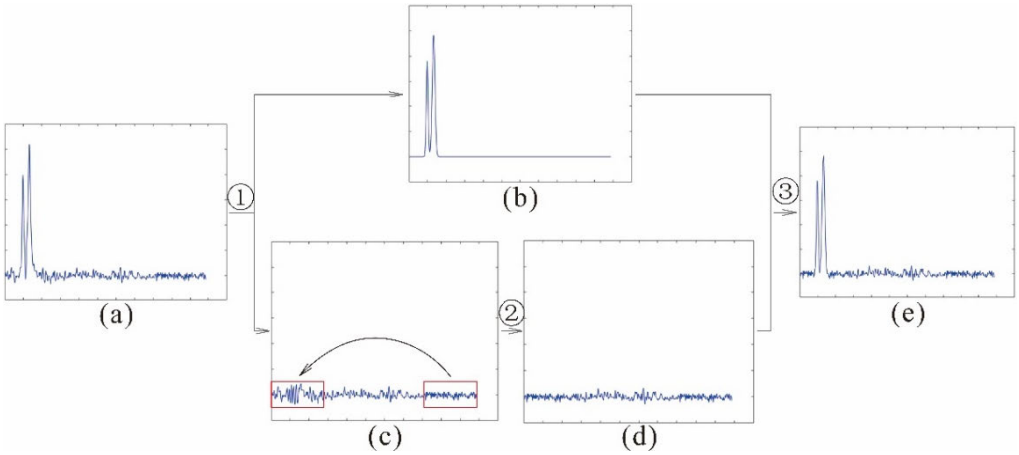

FIGURE 2. The process of simulating waveform. Step 1: Decompose the GLAS waveform (a) into signal components (b) and residual part (c). Step 2: Replace the part of residual part (c) which may contain effective signal to obtain simulated noise (d). Step 3: Superpose signal components (b) and simulated noise (d) to obtain simulated waveform (e).

B. DATA SIMULATION

Background noise is ubiquitous in the ICESat/GLAS data products, so it is necessary to remove its impacts. However, due to the absence of true data without noisy impacts, the filtering performance is hard to be quantitatively evaluated. The common ways to obtain the true values mainly include field measurement [20], extracting the elevation values from other sources of DEMs [37] and simulating GLAS waveforms [6], [14]. Among them, the evaluation by waveform simulation is easier to implement and generally applicable. Jutzi and Stilla [14] obtained the reference backscattered pulse by emitting pulse to a modeled surface. Duncanson *et al*. [6] used airborne discrete return LiDAR data to simulate GLAS waveforms.

In this paper, we obtain simulated waveforms by reforming GLAS waveform. The data simulation process is given in Figure. 2. Firstly, we decompose the GLAS waveform (Figure. 2(a)) into signal components (Figure. 2(b)) and residual part (Figure. 2(c)). Then, the signal components are used as the true value to generate the simulated waveform, and the residual part is regarded as background noise. However, part of the residual in Figure. 2(c) might contain part of effective signal. Thus, we use the residual in the flat part of waveform to replace the signal part with high amplitude, and construct the simulated noise (Figure. 2(d)). Finally, the signal components and simulated noise are superposed to obtain simulated waveform, as shown in Figure. 2(e). In this way, the simulated waveforms have the similar characteristics with the real GLAS waveforms, and the quantitative evaluation can be conducted using the waveform composed of the signal components (Figure. 2(b)) as the reference.

C. HP FILTERING AND l_1 TREND FILTERING

The piecewise adaptive-norm trend filtering method we proposed is on the basis of the idea of HP filtering and l_1 trend filtering [30, 31]. In trend filtering, the given scalar time series $y_t (t = 1, 2, \ldots, n)$, can be regarded as a composition of an underlying trend x_t and a randomly fluctuating component. The goal is to estimate the underlying trend and random component. The trend estimates x_t in H-P filtering is obtained

by minimizing the following function:

$$\min_x \left\{ (1/2) \sum_{t=1}^{n} (y_t - x_t)^2 + \lambda \sum_{t=2}^{n-1} (x_{t-1} - 2x_t + x_{t+1})^2 \right\} \quad (1)$$

where y_t is the obtained time series contaminated with noise, and x_t is the ideal smooth trend. The first term in Equation (1) is the data fidelity term measuring the residual, and the second term is a regular term depicting the smoothness of trend. The regularized parameter λ controls the trade-off between them. Kim [31] substituted the sum of absolute values for the sum of the squares of the quadratic difference of trend x_t and proposed l_1-*norm* regularized trend filtering, as below:

$$\min_x \left\{ (1/2) \sum_{t=1}^{n} (y_t - x_t)^2 + \lambda \sum_{t=2}^{n-1} |x_{t-1} - 2x_t + x_{t+1}| \right\} \quad (2)$$

The difference between HP filtering and l_1 trend filtering is that they use l_2 norm and l_1 norm in the regularization term respectively, which corresponds to different data characteristics in denoising. The main superiority of l_1-*norm* trend is that it produces piecewise linear result. Therefore, the signals expressed as abrupt changes in the estimated trend can be interpreted, while they tend to be smeared by HP filtering. However, HP filtering usually obtain a smooth result with noise clearly removed, while many unwanted noisy changes may also be reserved in the l_1 trend filtering. The performance varies with different norms assigned to the regularization term. The l_2 norm is prone to obtain over-smoothed results with smeared signal peaks, and the l_1 norm can maintain the feature points well together with some unnecessary noisy signals.

D. PROPOSED PIECEWISE ADAPTIVE-NORM TREND FILTERING

According to l_1 trend filtering and HP filtering, different norms can be used to constrain the smoothness variation of the estimated signal, and obtain results with different characteristics. These two methods can neither deal with the noise in the GLAS waveform, where the effective signals are concentrated in some parts and the other parts are basically noise. In order to address this problem, the adaptive norm is employed to balance the performance of results in smoothness and feature retention. We propose to adaptively assign different norm values for different parts of waveform, to combine the advantages of hybrid norms. We rewrite the HP filtering and l_1 trend filtering as one regularization model, which is:

$$\min_X \{ \| Y - X \|_p^p + \lambda \| DX \|_q^q \} \quad (3)$$

where Y is a time series or raw waveform in this paper, and X is the trend estimate or the filtered result. D is the second-order difference matrix, which results in a piecewise linear fitting. It has been proved that the second order difference regularization terms is more suitable for trend filtering, which is superior in maintaining the peak and valley than the third order difference regularization term [25]. λ is the regularization parameter used to control the smoothness of the results, and the results will be more smooth with a greater λ. For the data fidelity term, the l_2 norm-based ($p = 2$) linear least squares term is set in this study, due to that previous studies have manifested that the l_2 norm is effective for noise with Gaussian distribution [38]. It is therefore suitable for the noise distribution in GLAS waveform. For the regularization term, different q values ($q \in [1, 2]$) are applied according to the local signal energy. As illustrated before, l_2-*norm* has good performance in suppressing noise, and l_1-*norm* is superior to retaining the effective signal fluctuations [39]. For the GLAS waveforms, we employ the l_2-norm to constrain the smooth measures for the local parts with low signal strength, while a smaller norm is set for the local parts of the waveform superposed by noise and signal. A threshold t_q is defined to determine whether the local waveforms are mainly composed of background noise or effective echo energy, according to the previous studies [40]. The threshold t_q is calculated by the sum of the mean of background noise and the two standard variance noise:

$$t_q = m + 2 * \sigma \quad (4)$$

where m and σ represents the mean value and the standard deviation of the noise, respectively. These two variables are determined by the first or the last 100 values in the waveform, which usually contain little effective signal fluctuations in the waveforms [40]. The determination of the two parameters vary with the specific shape of GLAS waveforms. Such as the last 100 values in Figure. 1, it can be observed that these values generally do not contain effective information, so the t_q can represent the background level of the waveform. If the value in waveform is lower than t_q, it is the parts with low signal strength and is mainly composed by noise. Otherwise, if the value is higher than t_q, it is the parts superposed both by noise and effective echo energy. As a result, different norm can be assigned based on threshold t_q, which can effectively reflect the characteristics of GLAS waveform.

To further determine the optimal values of l_q-*norm* for the echoes containing signal of interest, we investigate the relationship between q values and the characteristics of GLAS waveform. The goal is to achieve the balance of removing the background noise and preserving the useful information. The root mean square errors (RMSEs) between the filtered results and the reference are used to evaluate the quality of the results.

1) THE RELATIONSHIP BETWEEN q AND WAVEFORM WIDTH

Due to the fact that waveform width of peak signal in GLAS data is varied depending on the surface features, it is necessary to explore the optimal q value for the data with different widths. Firstly, seven groups of single-peak data with different widths were simulated to explore the performance of different q values dealing with waveforms with different pulse widths. Each group contained 10 data composed of signal component with similar widths, and contaminated with

different levels of noise. From group 1 to group 7, the waveform widths become larger with the group number, and the mean group width of the signal peak ranged from about 25 to 107. The average RMSE are then obtained for each of the group test.

The results for data with different widths are shown in Figure.3. When the l_1-*norm* is adopted ($q = 1$), the smaller average RMSE values are obtained with smaller signal widths. As the value of q become larger ($\geq$1.4), we can get better denoising performance with large waveform widths. Moreover, the results are obviously unsatisfactory when the waveform width is relatively narrow. Overall, the filtering method can obtain the best performance when $q \in [1.1, 1.3]$, and the waveform width has little influence on the denoising effect.

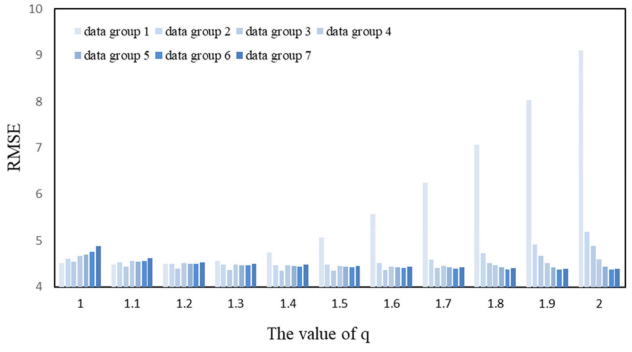

FIGURE 3. The relationship between *q* and waveform widths.

2) THE RELATIONSHIP BETWEEN *q* AND ENERGY INTENSITY

Ten groups of single-peak data were simulated to explore the properties of different q norms dealing with waveforms with different peak amplitude. The higher peak amplitude of the waveform indicates the higher energy of the return echo. Each group contained 10 single-peak data with similar peak amplitudes and different levels of noise, and the average RMSEs are then obtained. From group 1 to group 10, the signal energy increases with the group number.

The results are shown in Figure. 4. In general, the statistical results show that for the low-energy waveforms, better filtering results can be obtained with lager q. This is consistent with the previous description that smooth waveforms prefer a larger value of q to remove noise and avoid the artificial oscillations around the sharp edges. However, for the high-energy waveforms with large peak amplitude, the results show the opposite trend, where large values of q result in high RMSEs. For example, the RMSE values of data group 10 with $q = 2$ are much higher than the results with a relatively smaller value of q, such as the case of $q = 1.5$. The reason might be that l_2-*norm* results in the loss of useful signal energy, so the sharp peaks of waves are inclined to be preserved in those cases. In general, when $q \in [1.2, 1.5]$, the filtering method can balance the performance and obtain a pretty good result among all the waveform data with different energy intensity.

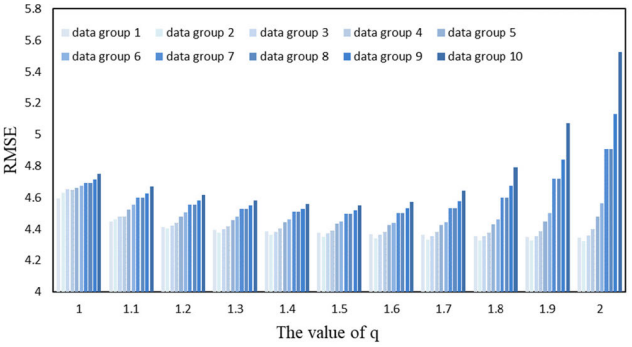

FIGURE 4. The relationship between q and the peak amplitude of waveforms.

3) THE RELATIONSHIP BETWEEN *q* AND GLAS WAVEFORM

To further test the robustness of q, 100 multi-peak data are simulated with different characteristics, including the numbers of wave peaks, amplitudes, and range distances. The simulated waveform data are contaminated with random noise with similar strength. Due to it is impossible to show a vast results, so only the average RMSEs are shown in Figure. 5. It can be observed that the adaptive-norm filtering method performs more robustly with a smaller value of q ($\leq$1.2) for multi-peak waveforms with different shapes and amplitudes.

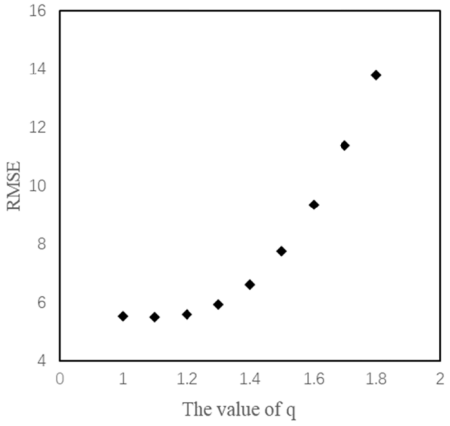

FIGURE 5. The relationship between *q* and complex waveforms.

Combining the optimal ranges of q value in the previous two experiments, we can conclude that the optimal q value is 1.2 for different GLAS waveform data with varied characteristics. The fractional norm applied here can obtain a moderate result, by clearly removing noise and minimizing the loss of useful signal simultaneously. As a result, the value of adaptive norm q can be finally determined. If the waveform value is lower than the threshold t_q, it is the parts with low signal strength and is mainly composed by noise, so the l_2-norm is used to smooth measures and suppress noise. Otherwise, if the value is higher than the threshold t_q, it is the parts superposed both by noise and signal, so a smaller norm of 1.2 is set to balance the noise removal and signal losses.

It can be expressed as:

$$q_i = \begin{cases} 2.0 & y_i \le t_q \\ 1.2 & y_i > t_q \end{cases} \quad (5)$$

where y_i is the photovoltaic value for each point, and q_i is the local norm assigned according to the threshold set in Equation (4). Therefore, the minimization function (3) can be rewritten as:

$$\min_x \left\{ \sum_{i=1}^{n} (y_i - x_i)_2^2 + \sum_{i=2}^{n-1} (|x_{i-1} - 2x_i + x_{i+1}|)^{q_i} \right\} \quad (6)$$

where x_i is the filtered result for the corresponding local point. In this paper, the hybrid-norm minimization function is solved by utilizing the iteratively reweighted norm (IRN) algorithm [41], which is easy to implement and efficient. For more details, it can be referred to the related materials [31], [39].

III. RESULTS

In the experiments, both simulated data and real GLAS waveforms are used to test the effectiveness of the proposed filtering algorithm. Four commonly used waveform filtering methods are chosen for the comparison, including the l_1 trend filtering, wavelet transform-based filtering, EMD and Gaussian filtering method.

A. EVALUATION INDEX

In order to quantitatively evaluate the denoising effect in the simulated experiments, evaluation indexes should be defined. In this paper, we evaluated the performance of the filtering methods not only by the filtered waveforms, but also by the components after decomposition to explore how denoising process will affect the subsequent information extraction.

1) EVALUATION FOR THE FILTERED WAVEFORM

Two indexes are used to evaluate the filtered waveforms, i.e. signal-to-noise ratio (SNR) and RMSE. The SNR is calculated as follows:

$$SNR = 10 \lg \left[\frac{\sum_{i=1}^{n} f_i^2}{\sum_{i=1}^{n} (s_i - f_i)^2} \right] \quad (7)$$

where s is the filtered waveform to be evaluated, and f is the noise-free waveform used as the reference. More details are described in the section of data simulation. The higher SNR and lower RMSE values indicate better performance of the filtering method.

For GLAS waveform, the most significant part is the effective echo signal. Therefore, in addition to analyzing the SNRs and RMSEs of the whole waveform, we also focus on the indexes of the partial wave containing effective echo energy. Therefore, there are four indicators employed to evaluate the filtering effect, including global RMSE (RMSE_G), global SNR (SNR_G), partial RMSE (RMSE_P) and partial SNR (SNR_P). The partial indexes are applied to evaluate the waves containing strong echo signal, which is determined as illustrated in Section II-D.

2) EVALUATION FOR THE COMPONENTS AFTER DECOMPOSITION

The goal of GLAS waveform filtering is to improve the accuracy of waveform decomposition and information extraction [36]. Thus, the RMSE statistics of the decomposed Signal components are used to evaluate the potential influence of the wave filtering to the component decomposition, which are defined as:

$$RMSE_D = \sum_{i=1}^{t} RMSE\_d_i \quad (8)$$

where $RMSE\_d_i$ is the RMSE value calculated by the *ith* signal component extracted from filtered waveform and the corresponding signal component of the reference waveform, and $RMSE_D$ is the sum of $RMSE\_d_i$ for the multi-peak waveforms with t signal components.

Gaussian decomposition is applied in this step to keep consistent with the decomposition method in data simulation (Section II-B), which is implemented with the Curve Fitting Tool in Matlab.

B. SIMULATED EXPERIMENTAL RESULTS

There are 10 single-peak data and 10 multi-peak data simulated to test the filtering methods. Except for the proposed piecewise adaptive-norm trend filtering method, four commonly used denoising methods for waveform data are incorporated for comparison. The parameters of each filtering method are adjusted to obtain the best error indexes through simulation experiments. For the wavelet transform, different wavelet bases were compared, and we adopted bior1.3 wavelet base to decompose the signal into 5 levels, and soft threshold to remove noise for each level. For Gaussian filtering, the different value of window width and the variance sigma were tested, and they are finally set as 5 and 2, respectively. For the EMD method, only the first noisy component is removed after the self-adaptively decomposing, to avoid more signal losses. For the regularized filtering methods, we have tuned lambda parameter to obtain the best quantitative or visual results in the experiments, both for the proposed method and the l_1 trend filtering method.

1) SINGLE-PEAK WAVEFORM

Table 1 shows four average evaluation indexes of the results obtained by five filtering methods in 10 single peak waveforms. It can be observed that the proposed filtering method has the best performance regarding all the indexes, with the highest SNR and lowest RMSE values. From the global indexes SNR_G and RMSE_G, the performance of wavelet transform is the second-best, followed by that of l_1 trend filtering, Gaussian filtering, and EMD. In terms of the partial indexes SNR_P and RMSE_P, l_1 trend filtering is slightly better than wavelet transform, and EMD still the last choice to use. Moreover, we give the error statistics of the decomposed waveforms, which imply the influence of the filtering process to the accuracy of decomposition. The differences between the two regularized trend filtering methods are relatively

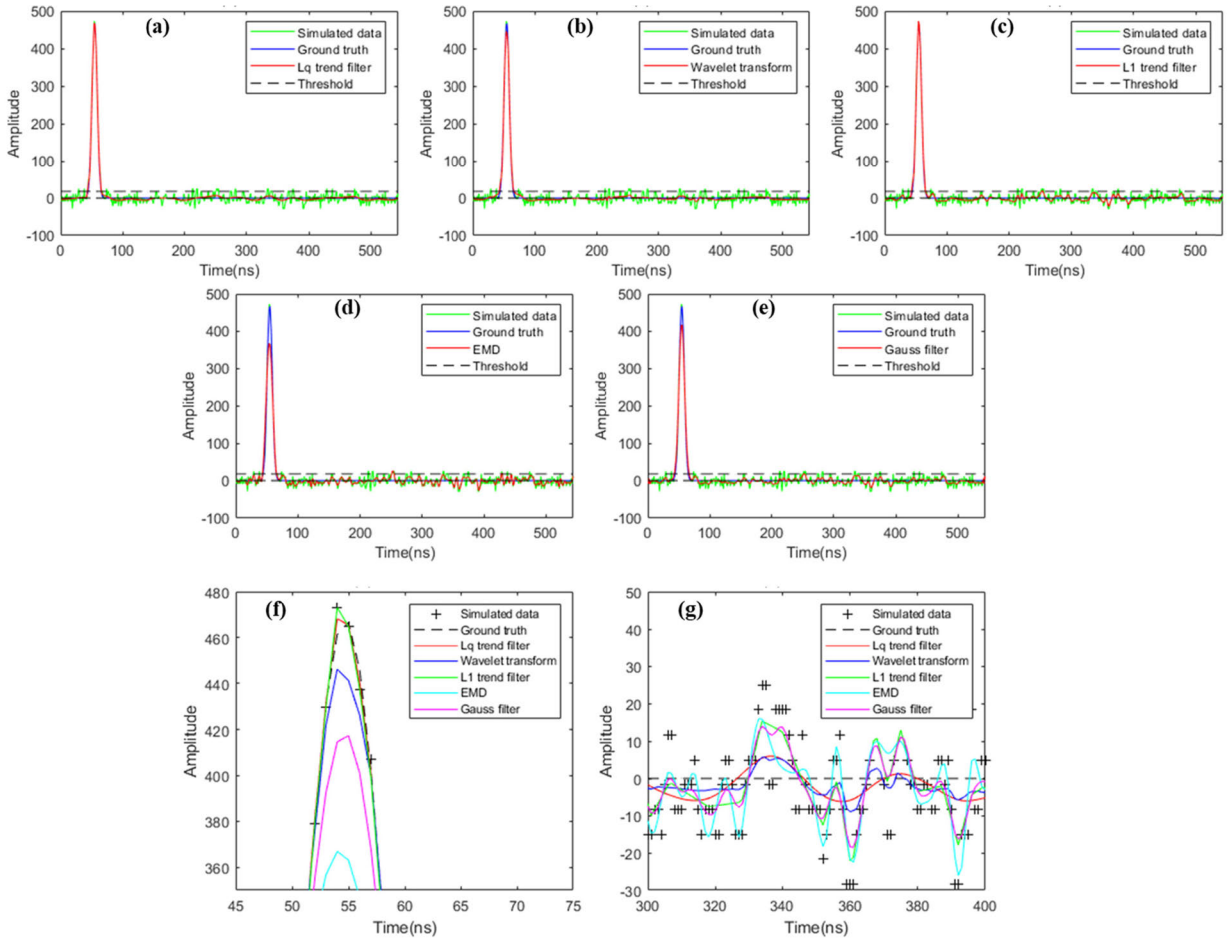

FIGURE 6. Results of four filtering methods applied to a sample single-peak waveform. (a)-(e) show the filtering results of the l_q trend filtering, wavelet transform, l_1 trend filtering, EMD, and Gaussian filtering method, respectively; and (f) and (g) are the zoomed view of the results to show the details of the peak and the flat parts in the waveform.

TABLE 1. Statistics of the evaluating indicators of 10 single-peak waveforms.

	Proposed	Wavelet	l_1 trend filtering	EMD	Gaussian filtering
SNR_G(dB)	24.829	23.175	21.152	9.470	14.470
SNR_ P(dB)	31.268	27.184	31.060	12.212	16.726
RMSE_G	3.232	3.774	5.209	19.603	10.027
RMSE_P	1.536	2.365	1.650	17.067	8.277
$RMSE_D$	0.639	2.374	0.890	65.432	8.724

TABLE 2. Statistics of the evaluating indicators of the sample single-peak waveform.

	Proposed	Wavelet	l_1 trend filtering	EMD	Gaussian filtering
SNR_G(dB)	23.362	21.871	19.115	11.498	16.483
SNR_P(dB)	31.776	27.252	31.212	13.342	20.244
RMSE_G	3.724	4.321	6.093	12.836	7.736
RMSE_P	1.411	2.320	1.505	10.245	4.984
$RMSE_D$	0.589	1.803	1.666	68.472	5.715

ignorable in this test for single-peak data. It indicates that both the l_1 and l_q trend filtering methods can obtain measurements with good quality on the flat terrain (with only one peak).

The visual performance of five methods applied to a sample single-peak waveform was also presented in Figure. 6, and the evaluation indexes of this data are shown in Table 2. It can be observed that Gaussian filtering and EMD causes significant energy loss for the wave peak, while retaining much noise for the low-energy part of the waveform. This is the reason for the unsatisfied quantitative statistics of the Gaussian filtering and EMD methods. The main advantage of l_1 trend filter is the preservation of peak energy, but it also preserves too much noise. Both wavelet filter and the proposed l_q trend filter can well suppress the background noise. However, energy loss at the wave peak can be observed in the results of wavelet filter.

Combining the quantitative and the qualitative results, we can come to the conclusion that the proposed l_q trend filtering is superior than other four methods in the processing

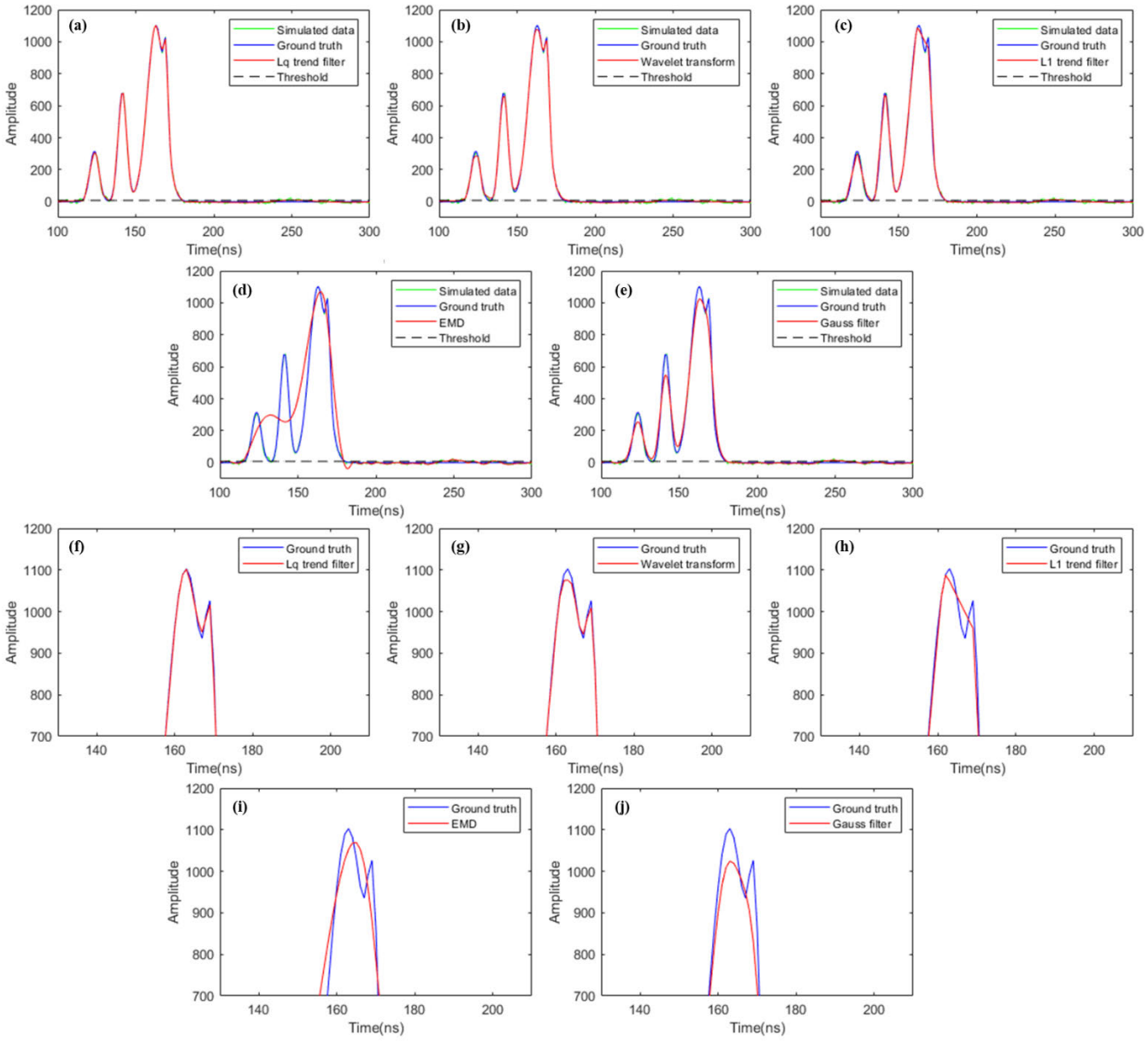

FIGURE 7. Results of four filtering methods applied to a multi-peak waveform. (a)-(e) show the filtering results of the l_q trend filtering, wavelet transform, l_1 trend filtering, EMD and Gaussian filtering method, respectively; (f)-(j) are the zoomed view of the five results in the peak.

of the single peak waveform. The threshold t_q can distinguish the different parts of the waveform, and the adaptive norm can achieve the goal of removing the noise with little energy loss and preserving the waveform's shape. However, the EMD, Gaussian and wavelet based filtering are prone to significantly underestimate the peak amplitude, and obtain the oversmoothed waveform. As the peak amplitude is one of the key parameters for ground peak location and cover classification [42], [43], the capability to preserve the echo energy is significant to judge a filtering method. Both the l_1 trend filter and the proposed l_q trend filter obtain results with sharp peaks. However, the resulting signal of l_1 trend filter remains too much noise, especially over the low-energy parts.

2) MULTI-PEAK WAVEFORM

ICESat GLAS waveforms are classified according to the characteristics of the terrain and surface coverage within the footprints. The single-peak data generally represent the waveforms over flat barren land. However, in the general cases, there are more than one echoes from the ground with rugged topography and objects (e.g. vegetation and buildings) covered [6]. For waveforms with three or more peaks,

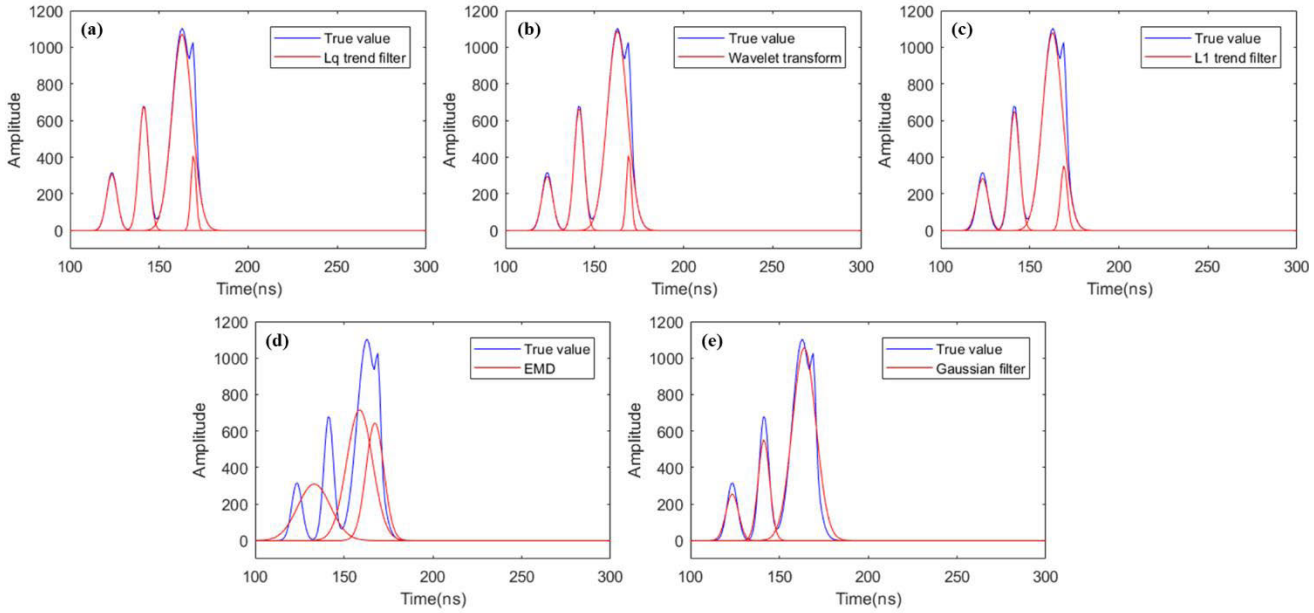

FIGURE 8. Results of decomposed multi-peak waveforms, the red line is the signal component of different results and the blue line is the true value. (a)-(e) show the decomposed results of the l_q trend filtering, wavelet transform, l_1 trend filtering, EMD and Gaussian filtering method, respectively.

as shown in Figure. 1(b), the filtering become more complex. In this section, we test the performance of the methods on complex GLAS waveforms on 10 simulated multi-peak data.

The mean quantitative results are given in Table 3. It can be found that EMD and Gaussian filtering method is not capable of processing data with complex shapes, where large RMSEs and low SNRs are obtained. Wavelet-based filter has better performance than l_1 trend filtering in this case, in terms of both the global indexes (SNR_G and RMSE_G) and the partial indexes (SNR_P and RMSE_P). The proposed piecewise adaptive-norm trend filtering is still the best among the five filtering methods. Due to the varied peak numbers, the mean statistics after waveform decomposition are not presented here.

TABLE 3. Statistics of decomposition results of 10 multi-peak waveforms.

	Proposed	Wavelet	l_1 trend filtering	EMD	Gaussian filtering
SNR_G (dB)	31.095	28.951	26.763	7.657	16.050
SNR_P (dB)	33.612	30.430	28.160	7.756	16.243
RMSE_G	4.079	5.099	6.890	61.370	21.628
RMSE_P	3.039	4.289	6.008	60.207	21.185

The visual comparison results for a sample of four-peak waveform are presented in Figure. 7. The third and the fourth peak are close to each other and have similar amplitudes, which makes it easy to be smeared after filtering. It can be observed from Figure. 7 (c) that the signal form between the closely neighboring peaks is failed to retain the original wave structure in l_1 trend filter. This is probably caused by the strict constraints of l_1-*norm*. Due to the last two peaks are too close, the one with lower amplitude are scarified by the l_1 trend filter to get the sharp features. Moreover, EMD and Gaussian filter significantly over smooth the peak of the waveform, which is similar with the single-peak data tests. From the zoomed view shown in Figure. 7 (f-j), more details can be observed. The wavelet filtering and the proposed method can preserve the basic form of the waveform. However, the wavelet transform-based method apparently underestimates the peak amplitudes, which resulted in unsatisfactory quantitative results.

For complex waveforms, the loss of peak energy and signal distortion in denoising might lead to decomposition errors. Therefore, the results after decomposition were compared in Figure. 8. It can be seen that the waveform filtered by EMD and Gaussian filtering even causes one signal component lost, and all the components of EMD results have obviously shift to the true value. In addition, the amplitude of the corresponding Signal component of the results of l_1 trend filtering is much smaller than that of the other two methods. Moreover, we calculate the quantitative evaluation results for both the filtered waveforms and the decomposed Signal components, as shown in Table 4. It can be analyzed that the

TABLE 4. Statistics of decomposition results of a sample multi-peak waveforms.

	Proposed	Wavelet	l_1 trend filtering	EMD	Gaussian filtering
SNR_G(dB)	31.949	31.016	25.479	8.772	18.459
SNR_P(dB)	35.436	32.988	26.116	8.802	18.666
RMSE_G	5.548	6.140	11.612	84.175	24.707
RMSE_P	3.713	4.892	10.788	83.843	24.116

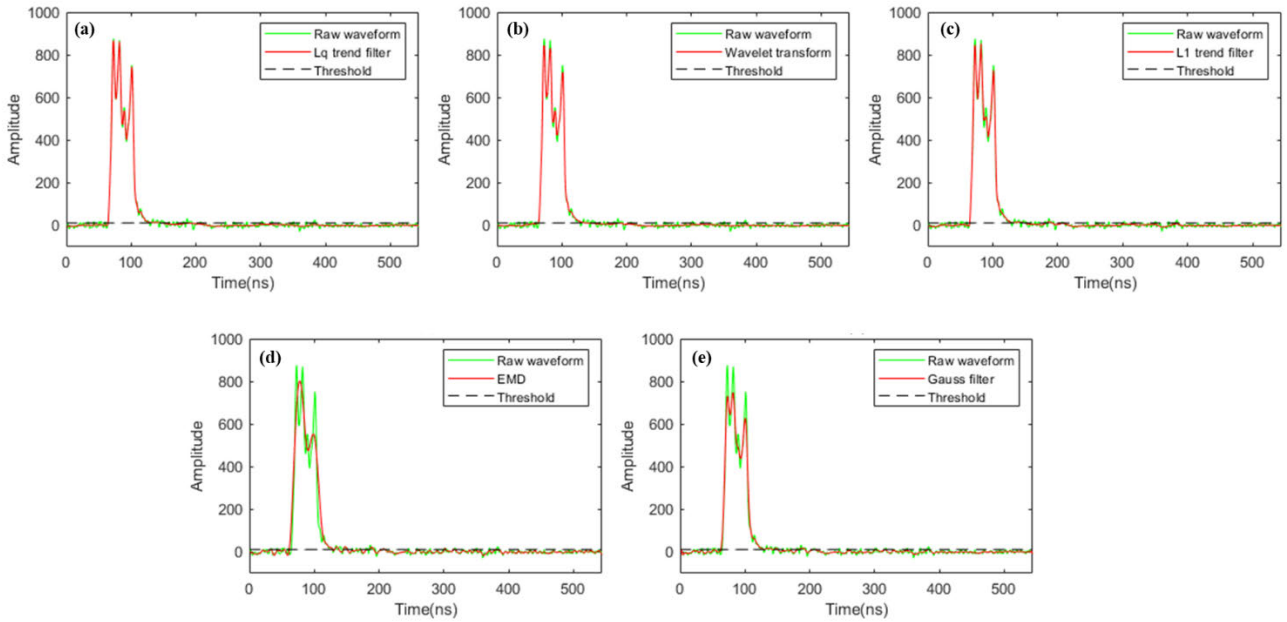

FIGURE 9. Filtering results of the real GLAS waveform. (a)-(e) show the filtering results of the l_q trend filtering, wavelet transform, l_1 trend filtering, EMD and Gaussian filtering method, respectively.

l_q trend filtering outperforms the wavelet-based algorithm in terms of the preservation of peak amplitude and waveform structure.

Considering the experiments on both single-peak and multi-peak waveforms, the results show that the piecewise adaptive-norm trend filtering exhibits a better performance compared to other four methods. The advantages of the proposed method in maintaining peak amplitude are vital to extract the reflective information. Moreover, the ability to keep waveform structure can lead to more accurate identification of peak number for complex signals.

C. REAL DATA EXPERIMENTS

To verify the performance of the proposed method on real data, we also conduct experiments on real GLAS waveforms. In Figure. 9, we present the filtering results for a sample multi-peak waveform. This is a four-peak waveform retrieved from GLA01 product list, where the distances between the neighboring peaks are very close. Moreover, the amplitude of the third peak is much smaller than the other three peaks. Therefore, the filtering is a difficult task as the structure of the sample waveform is very complex. From the results, it can be seen that the Gaussian filter smear the third peak, and the EMD result even smear two peaks. Although the wavelet transform and l_1 trend filtering method preserves all the peaks, the amplitudes are obviously underestimated. In the results of the proposed method, the peak amplitudes are well retained and the background noise is effectively suppressed. The filtered waveform is smooth and the shape structure is clear.

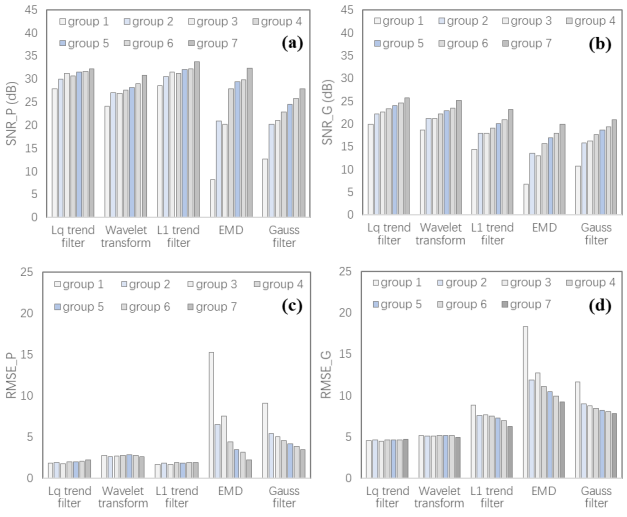

FIGURE 10. The filtering performance for the waveforms with different widths. The waveform widths increase from group 1 to group 7. (a) and (c) show the mean partial evaluation indexes for the results of different methods, while (b) and (d) present the mean global SNRs and RMSEs.

IV. DISCUSSION

The results above indicate that the proposed method can obtain much better results than the other four comparison methods, both in the qualitative and quantitative evaluations. The threshold t_q can also well identify the different parts in waveform, and the adaptive norm could effectively remove noise and avoid loss of signal details. In order to explore the denoising characteristics of filtering methods on different waveform features, the influence of waveform width and energy intensity are further discussed.

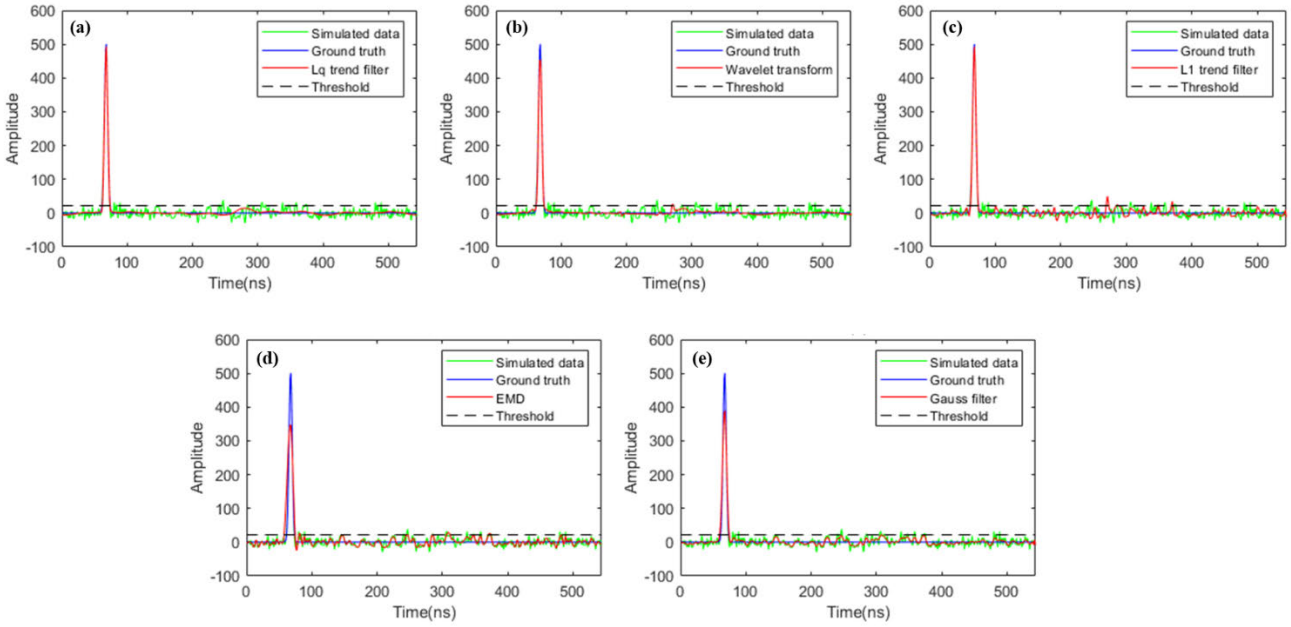

FIGURE 11. Filtering results of a narrow waveform. (a)-(e) show the filtering results of the l_q trend filtering, wavelet transform, l_1 trend filtering, EMD and Gaussian filtering method, respectively.

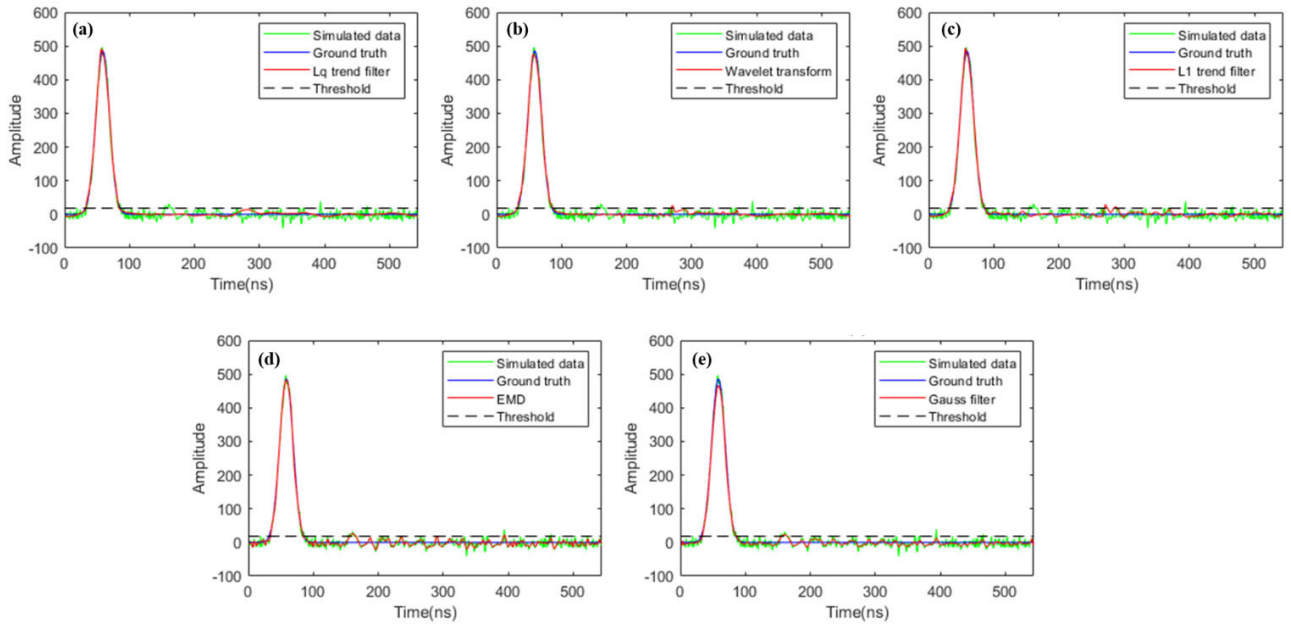

FIGURE 12. Filtering results of a wide waveform. (a)-(e) show the filtering results of the l_q trend filtering, wavelet transform, l_1 trend filtering, EMD and Gaussian filtering method, respectively.

A. WAVEFORMS WITH DIFFERENT WAVEFORM WIDTHS

Similar with the settings in Section 2-D-1, seven groups single-peak waveforms are simulated. Each group contains 10 waveforms composed of the same Signal component, and contaminated with different levels of noise. From group 1 to group 7, the waveform widths become larger with the group number. The average RMSE are then obtained for each of the group test.

Figure. 10 shows the evaluation for the results of five filtering methods. It can be seen that EMD, Gaussian and l_1 trend filtering are sensitive to impulse width. The effects of the three methods are mostly positively correlated with the

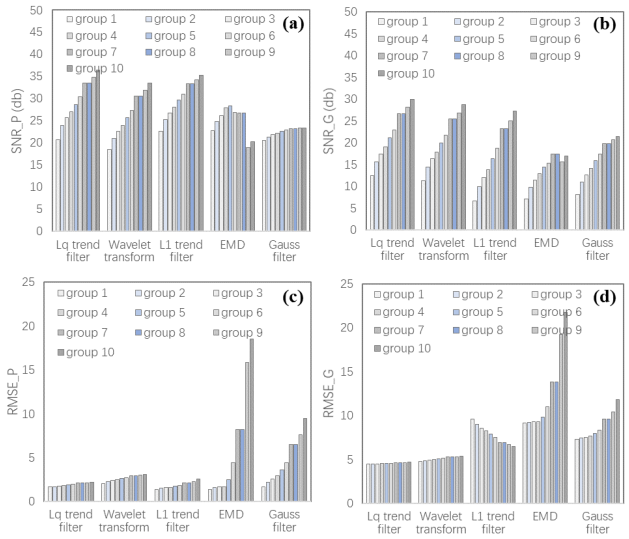

FIGURE 13. Effect of waveform energy on denoising. The wave energy intensity increases from group 1 to group 10. (a) and (c) show the mean partial evaluation indexes for the results of different methods, while (b) and (d) present the mean global SNRs and RMSEs.

waveform widths. It means that they obtain better filtering results for the waveforms with larger widths. Especially the EMD could get a better result than the Gaussian filtering in the data with large widths, but with poorer results in the data with small widths. Comparatively, the wavelet-based and the l_q trend filtering are robust in processing waveforms with different widths.

To explore the reasons for this phenomenon, the filtering results for a narrow waveform and a wide waveform are presented in Figure. 11 and Figure. 12, respectively. It can be found that the peak underestimation of EMD and Gaussian filter significantly degrades the quality of filtered result. The EMD is even poorer than Gaussian filter in the narrow sample waveform, but it is much better in the wide sample waveform. The simple filtering method based on Gaussian smooth kernel and self-adaptively decomposition has difficulty in processing the waveform with a sharp echo peak, which results in poor assessment. In terms of the l_1 trend filtering, the remaining background noise in the low-energy part of the waveform is the main reason for the unstable evaluation results. The wavelet transform-based filter and the l_q trend filtering are not sensitive to the waveform width. Moreover, the l_q trend filtering outperforms the wavelet filtering both in the noise suppression and the details preservation.

B. WAVEFORMS WITH DIFFERENT ENERGY INTENSITY

Finally, the filtering performance regarding the energy intensity is discussed. Ten groups of single-peak waveforms are simulated. Each group contains 10 waveforms composed of the same signal component, and contaminated with different levels of noise. The wave energy intensity increases from group 1 to group 10. The results are shown in Figure. 13.

The SNR values should be increased along with the energy intensity. However, the gently varied values of SNR_P for the results of Gaussian filter imply the significant loss of signal energy, and the SNR of EMD result even decreased in the data with high energy intensity. The RMSE values

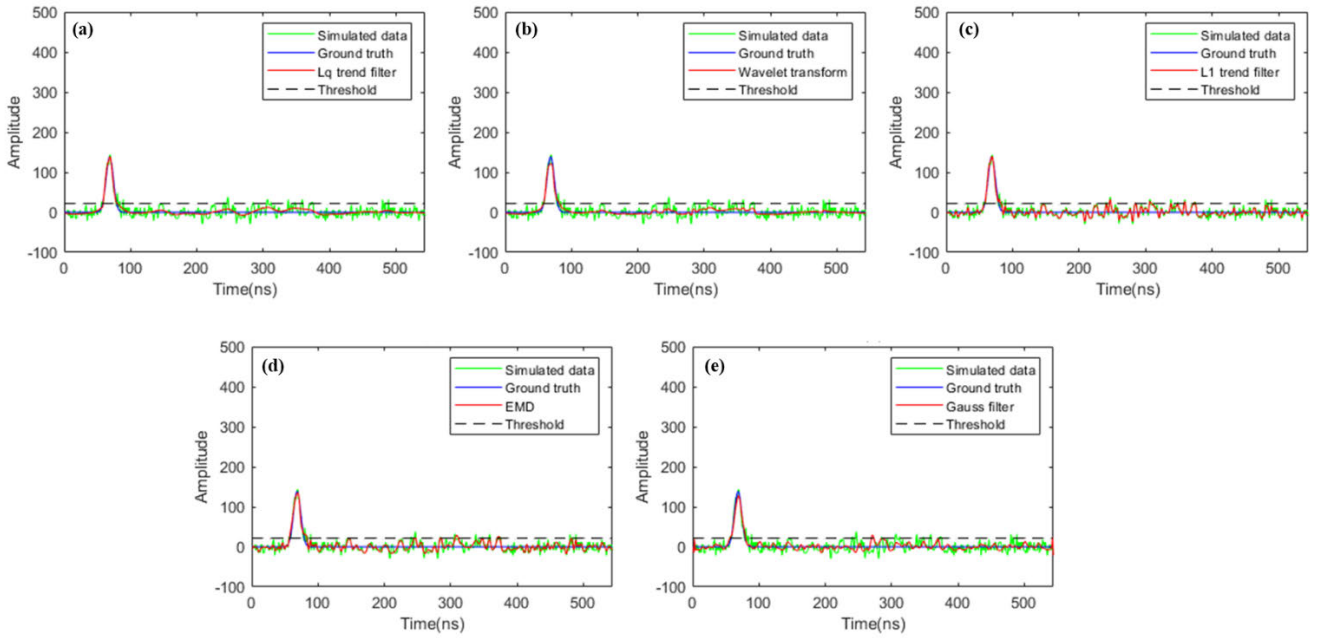

FIGURE 14. Denoising results of low peak energy data. (a)-(e) show the filtering results of the l_q trend filtering, wavelet transform, l_1 trend filtering, EMD and Gaussian filtering method, respectively.

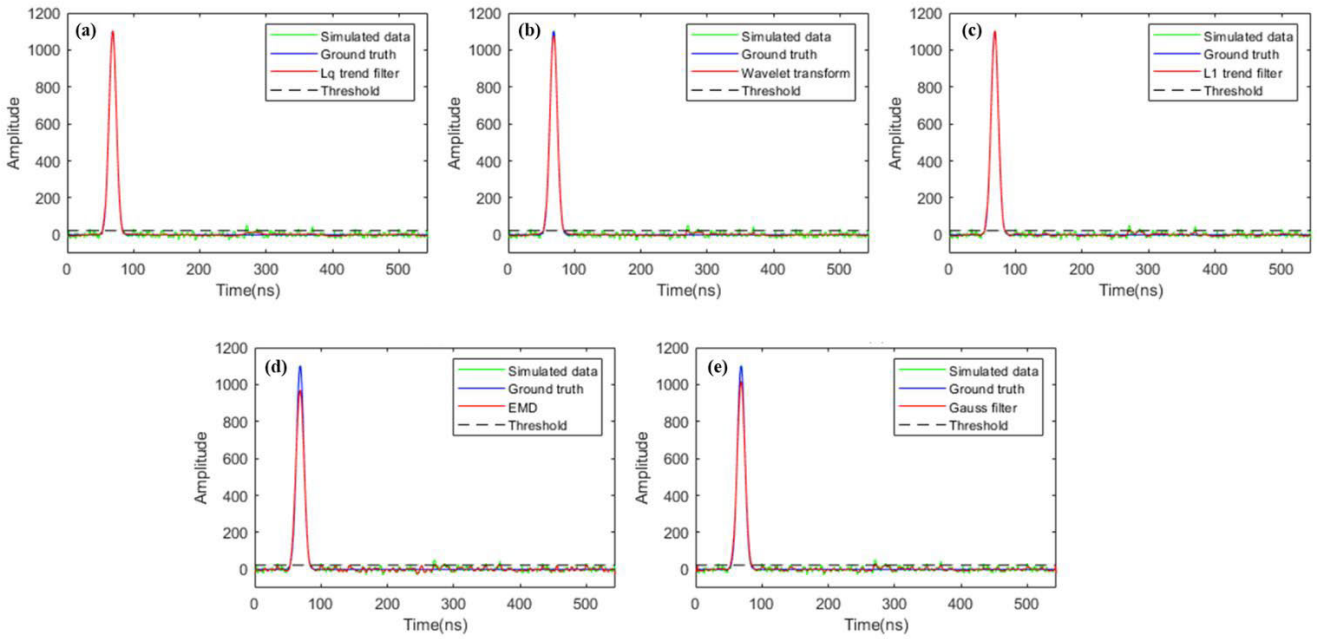

FIGURE 15. Denoising results of high peak energy data. (a)-(e) show the filtering results of the l_q trend filtering, wavelet transform, l_1 trend filtering, EMD and Gaussian filtering method, respectively.

further verify the poor performance of EMD and Gaussian filtering method, especially the result of EMD in data with high energy intensity. Among the other three methods, the l_1 trend filtering can obtain good results for the peak part; unfortunately, it remains too much noise, thus affects the overall evaluation results. Similar with the previous cases, the proposed adaptive-nor l_q trend filtering achieves best SNR and RMSE values. Furthermore, the RMSE values demonstrates the robustness of the proposed method for waveforms with different peak amplitudes.

Figure. 14 and Figure. 15 show the denoising results of five filtering methods on data with low and high peak amplitudes, respectively. From the visual results, the properties of different methods can be clearly observed. Generally, the l_1 trend filtering can obtain good results in the cases where the peak amplitude is far larger than the noise level. However, it might fail to process the waveforms with relatively low peak amplitude. Combining the advantages of hybrid norms using the adaptive strategy, the proposed l_q trend filtering overcomes the problem of l_1 trend filtering and improves the filtering performance.

V. CONCLUSION

To improve the accuracy of waveform filtering, we propose a piecewise adaptive-norm trend filtering method to take advantages of different norms (l_q-*norm*, $q \in [1, 2]$) in the regularized framework. The goal of the adaptive-norm filtering method is to reduce the smoothness of the effective signal, while suppressing background noise as much as possible. The effectiveness of the proposed method is tested with simulated data and real data. In the simulated experiments, the filtered results are evaluated after denoising and waveform decomposition. The results verify that the method was superior to the other three commonly used GLAS waveform filtering methods, i.e. Gaussian filtering, wavelet transform, EMD and l_1 trend filtering methods. It is also indicated that the proposed method performs well in retain the peak amplitude and the structure of the waveform while removing noise, even for the waveforms with complex shapes. Thus, it can improve the potential accuracy of GLAS-derived parameters, e.g. ground peak location, reflective information, and range distance, which makes significant sense in the related geoscience applications.

REFERENCES

[1] B. E. Schutz, H. J. Zwally, C. A. Shuman, D. Hancock, and J. P. DiMarzio, "Overview of the ICESat mission," *Geophys. Res. Lett.*, vol. 32, no. 21, 2005.

[2] X. Wang, X. Cheng, P. Gong, H. Huang, Z. Li, and X. Li, "Earth science applications of ICESat/GLAS: A review," *Int. J. Remote Sens.*, vol. 32, no. 23, pp. 8837–8864, Aug. 2011.

[3] C. A. Shuman, H. J. Zwally, B. E. Schutz, A. C. Brenner, J. P. DiMarzio, V. P. Suchdeo, and H. A. Fricker, "ICESat antarctic elevation data: Preliminary precision and accuracy assessment," *Geophys. Res. Lett.*, vol. 33, no. 7, Apr. 2006.

[4] NSIDC. (2017). *What is the Accuracy of GLAS Elevation Measurements?* [Online]. Available: https://nsidc.org/support/21801268-How-does-surface-roughness-affect-the-accuracy-of-the-elevation-measurement

[5] W. Abdalati, H. J. Zwally, R. Bindschadler, B. Csatho, S. L. Farrell, H. A. Fricker, D. Harding, R. Kwok, M. Lefsky, T. Markus, A. Marshak, T. Neumann, S. Palm, B. Schutz, B. Smith, J. Spinhirne, and C. Webb, "The ICESat-2 laser altimetry mission," *Proc. IEEE*, vol. 98, no. 5, pp. 735–751, May 2010.

[6] L. I. Duncanson, K. O. Niemann, and M. A. Wulder, "Estimating forest canopy height and terrain relief from GLAS waveform metrics," *Remote Sens. Environ.*, vol. 114, no. 1, pp. 138–154, Jan. 2010.

[7] S. Ghosh, S. Nandy, S. Patra, S. P. S. Kushwaha, A. Senthil Kumar, and V. K. Dadhwal, "Land cover classification using ICESat/GLAS full waveform data," *J. Indian Soc. Remote Sens.*, vol. 45, no. 2, pp. 327–335, Apr. 2017.
[8] L. N. Connor, S. L. Farrell, D. C. McAdoo, W. B. Krabill, and S. Manizade, "Validating ICESat over thick sea ice in the northern canada basin," *IEEE Trans. Geosci. Remote Sens.*, vol. 51, no. 4, pp. 2188–2200, Apr. 2013.
[9] D. Felikson, T. J. Urban, B. C. Gunter, N. Pie, H. D. Pritchard, R. Harpold, and B. E. Schutz, "Comparison of elevation change detection methods from ICESat altimetry over the greenland ice sheet," *IEEE Trans. Geosci. Remote Sens.*, vol. 55, no. 10, pp. 5494–5505, Oct. 2017.
[10] W. Liao, F. Van Coillie, L. Gao, L. Li, B. Zhang, and J. Chanussot, "Deep learning for fusion of APEX hyperspectral and full-waveform LiDAR remote sensing data for tree species mapping," *IEEE Access*, vol. 6, pp. 68716–68729, Nov. 2018.
[11] S. Nie, C. Wang, P. Dong, G. Li, X. Xi, P. Wang, and X. Yang, "A novel model for terrain slope estimation using ICESat/GLAS waveform data," *IEEE Trans. Geosci. Remote Sens.*, vol. 56, no. 1, pp. 217–227, Jan. 2018.
[12] X. Li, K. Xu, and L. Xu, "Surface slope and roughness measurement using ICESat/GLAS elevation and laser waveform," *Meas. Sci. Technol.*, vol. 27, no. 9, Aug. 2016, Art. no. 095202.
[13] J. Wu, J. A. N. van Aardt, J. McGlinchy, and G. P. Asner, "A robust signal preprocessing chain for small-footprint waveform LiDAR," *IEEE Trans. Geosci. Remote Sens.*, vol. 50, no. 8, pp. 3242–3255, Aug. 2012.
[14] B. Jutzi and U. Stilla, "Range determination with waveform recording laser systems using a Wiener filter," *ISPRS J. Photogramm. Remote Sens.*, vol. 61, no. 2, pp. 95–107, Nov. 2006.
[15] F. Pirotti, "IceSAT/GLAS waveform signal processing for ground cover classification: State of the art," *Italian J. Remote Sens.*, vol. 42, no. 2, pp. 13–26, Sep. 2010.
[16] G. Deng, D. B. H. Tay, and S. Marusic, "A signal denoising algorithm based on overcomplete wavelet representations and Gaussian models," *Signal Process.*, vol. 87, no. 5, pp. 866–876, May 2007.
[17] C. E. Parrish, "Exploiting full-waveform lidar data and multiresolution wavelet analysis for vertical object detection and recognition," in *Proc. IEEE Int. Geosci. Remote Sens. Symp.*, Barcelona, Spain, Jul. 2007, pp. 2499–2502.
[18] Q. Sai, X. Yanqiu, L. Licun, and W. Meng, "ICESAT-GLAS data processing based on wavelet transform," *Forest Eng.*, vol. 5, May 2012.
[19] M. Azadbakht, C. S. Fraser, C. Zhang, and J. Leach, "A signal denoising method for full-waveform LiDAR data," in *Proc. ISPRS Ann.*, Antalya, Turkey, 2013, pp. 11–13.
[20] I. A. Iqbal, J. Dash, S. Ullah, and G. Ahmad, "A novel approach to estimate canopy height using ICESat/GLAS data: A case study in the new forest national park, UK," *Int. J. Appl. Earth Observ. Geoinf.*, vol. 23, pp. 109–118, Aug. 2013.
[21] A. A. Borsa, H. A. Fricker, and K. M. Brunt, "A terrestrial validation of ICESat elevation measurements and implications for global reanalyses," *IEEE Trans. Geosci. Remote Sens.*, vol. 57, no. 9, pp. 6946–6959, Sep. 2019.
[22] C. N. Babu and B. E. Reddy, "A moving-average filter based hybrid ARIMA–ANN model for forecasting time series data," *Appl. Soft Comput.*, vol. 23, pp. 27–38, Oct. 2014.
[23] E. S. Gardner, "Exponential smoothing: The state of the art," *J. Forecasting*, vol. 4, no. 1, pp. 1–28, Sep. 1985.
[24] A. Jaeger, "Mechanical detrending by hodrick-prescott filtering: A note," *Empirical Econ.*, vol. 19, no. 3, pp. 493–500, Sep. 1994.
[25] S. J. Kim, K. Koh, S. Boyd, and D. Gorinevsky, "ℓ_1 trend filtering," *SIAM Rev.*, vol. 51, no. 2, pp. 339–360, May 2009.
[26] N. E. Huang, Z. Shen, S. R. Long, M. C. Wu, H. H. Shih, Q. Zheng, N.-C. Yen, C. C. Tung, and H. H. Liu, "The empirical mode decomposition and the Hubert spectrum for nonlinear and non-stationary time series analysis," *Proc. Roy. Soc. A, Math. Phys. Eng. Sci.*, vol. 454, no. 1971, pp. 903–995, Mar. 1998.
[27] S. Wu, Z. Liu, and B. Liu, "Enhancement of lidar backscatters signal-to-noise ratio using empirical mode decomposition method," *Opt. Commun.*, vol. 267, no. 1, pp. 137–144, Nov. 2006.
[28] I. Daubechies, J. Lu, and H.-T. Wu, "Synchrosqueezed wavelet transforms: An empirical mode decomposition-like tool," *Appl. Comput. Harmon. Anal.*, vol. 30, no. 2, pp. 243–261, Mar. 2011.
[29] M. Li, L.-H. Jiang, and X.-L. Xiong, "A novel EMD selecting thresholding method based on multiple iteration for denoising LIDAR signal," *Opt. Rev.*, vol. 22, no. 3, pp. 477–482, May 2015.
[30] J. Chang, L. Zhu, H. Li, F. Xu, B. Liu, and Z. Yang, "Noise reduction in lidar signal using correlation-based EMD combined with soft thresholding and roughness penalty," *Opt. Commun.*, vol. 407, pp. 290–295, Jan. 2018.
[31] Y.-X. Wang, J. Sharpnack, A. Smola, and R. J. Tibshirani, "Trend filtering on graphs," *J. Mach. Learn. Res.*, vol. 17, no. 1, pp. 3651–3691, Jan. 2016.
[32] T. Poggio, V. Torre, and C. Koch, "Computational vision and regularization theory," *Nature*, vol. 317, no. 6035, pp. 314–319, Sep. 1985.
[33] L. Yue, H. Shen, Q. Yuan, and L. Zhang, "A locally adaptive L1–L2 norm for multi-frame super-resolution of images with mixed noise and outliers," *Signal Process.*, vol. 105, pp. 156–174, Dec. 2014.
[34] Y. Meng, Z. Zhou, Y. Liu, and Q. Luo, "Adaptive pseudo-p-norm regularization based de-speckling of SAR images," *Remote Sens. Lett.*, vol. 9, no. 12, pp. 1177–1185, Dec. 2018.
[35] G. Sun, K. Ranson, D. Kimes, J. Blair, and K. Kovacs, "Forest vertical structure from GLAS: An evaluation using LVIS and SRTM data," *Remote Sens. Environ.*, vol. 112, no. 1, pp. 107–117, Jan. 2008.
[36] C. Wang, F. Tang, L. Li, G. Li, F. Cheng, and X. Xi, "Wavelet analysis for ICESat/GLAS waveform decomposition and its application in average tree height estimation," *IEEE Geosci. Remote Sens. Lett.*, vol. 10, no. 1, pp. 115–119, Jan. 2013.
[37] D. J. Harding, "ICESat waveform measurements of within-footprint topographic relief and vegetation vertical structure," *Geophys. Res. Lett.*, vol. 32, no. 21, Oct. 2005.
[38] D. Bertaccini, R. H. Chan, S. Morigi, and F. Sgallari, "An adaptive norm algorithm for image restoration," in *Proc. SSVM*, Berlin, Germany, 2011, pp. 194–205.
[39] H. Shen, L. Peng, L. Yue, Q. Yuan, and L. Zhang, "Adaptive norm selection for regularized image restoration and super-resolution," *IEEE Trans. Cybern.*, vol. 46, no. 6, pp. 1388–1399, Jun. 2016.
[40] M. A. Lefsky, D. J. Harding, M. Keller, W. B. Cohen, C. C. Carabajal, F. Del Bom Espirito-Santo, M. O. Hunter, and R. de Oliveira, "Estimates of forest canopy height and aboveground biomass using ICESat," *Geophys. Res. Lett.*, vol. 32, no. 22, Nov. 2005.
[41] B. Wohlberg and P. Rodriguez, "An iteratively reweighted norm algorithm for minimization of total variation functionals," *IEEE Signal Process. Lett.*, vol. 14, no. 12, pp. 948–951, Dec. 2007.
[42] C. Hilbert and C. Schmullius, "Influence of surface topography on ICESat/GLAS forest height estimation and waveform shape," *Remote Sens.*, vol. 4, no. 8, pp. 2210–2235, Jul. 2012.
[43] E. Khalefa, I. P. J. Smit, A. Nickless, S. Archibald, A. Comber, and H. Balzter, "Retrieval of savanna vegetation canopy height from ICESat-GLAS spaceborne LiDAR with terrain correction," *IEEE Geosci. Remote Sens. Lett.*, vol. 10, no. 6, pp. 1439–1443, Nov. 2013.

LIANYING LI was born in Da'an, Jilin, China, in 1974. He received the B.S. degree in cartography from the Former Wuhan Technical University of Surveying and Mapping, and the M.S. degree in cartography and geographical information system and the Ph.D. degree in cartography and geographical information engineering from Wuhan University, Wuhan, China, in 2002 and 2008, respectively. From 2000 to 2008, he was a Lector with the School of Resource and Environmental Sciences, Wuhan University. Since 2009, he has been an Assistant Professor with the School of Resource and Environmental Sciences, Wuhan University. He is the author of three books and more than ten articles. His research interests include map projection, geographical information engineering, and 3D laser scanner.

MENGRONG CAI was born in Jingmen, Hubei, China, in 1995. She received the B.S. and M.S degrees from Wuhan University, Wuhan, Hubei, in 2017 and 2019, respectively. From 2013 to 2017, she majored in geographic information science and cartography, also took participate in National Atlas Project in the last two years. In the period of postgraduate study, she worked on data denoising for fullwave lidar (e.g. ICESAT/GLAS) and came up with a filtering method based on trend filtering. She is currently working on mobile detective Lidar as an Algorithm Engineer in RoboSense after getting M.S degree.

XIAOBIN GUAN was born in Ganzhou, Jiangxi, China, in 1993. He received the B.S. and Ph.D. degrees in geographical information system from the School of Resource and Environmental Sciences, Wuhan University, Wuhan, Hubei, China, in 2013 and 2018, respectively. He is currently a Postdoctoral Research Assistant with the School of Resource and Environmental Sciences, Wuhan University. His research interests include data filtering, remote sensing image processing, application of remote sensing data in the terrestrial ecosystem, and global change.

DONG CHU was born in Luan, Anhui, China, in 1996. He received the B.S. degree from Northwest A&F University, Yangling, Shaanxi, China, in 2018. He is currently pursuing the Ph.D. degree with the School of Resource and Environmental Sciences, Wuhan University, Wuhan, China. His research interests include time series data filtering, remote sensing image restoration, hyperspectral image data processing, and low rank matrix/tensor representation.